# Magnetic Flux-Line Lattices and Vortices in the Copper Oxide Superconductors

D. J. BISHOP, P. L. GAMMEL, D. A. HUSE, C. A. MURRAY

**A variety of recent experiments on both the static and the dynamic properties of vortices and flux-line lattices in the mixed state of the copper oxide superconductors are discussed. The experiments are of two basic types: (i) experiments that image the magnetic flux patterns either with magnetic decoration or neutrons and give information about static structures, and (ii) experiments that explore the dynamics of vortices either through the resistivity or other electrodynamic responses of the material. Results of these experiments argue in favor of the existence of a true phase transition in the high-field vortex state from a low-temperature superconducting vortex glass phase into a disordered high-temperature vortex fluid phase. The vortex glass phase transition model does a good job of explaining high-precision measurements of the dynamics at the transition. At low fields and temperatures, very long range hexatic order in the flux-line lattice is observed.**

THE BEHAVIOR OF SUPERCONDUCTORS IN THE PRESENCE OF a magnetic field has been the subject of much scientific, as well as practical, interest over the past few decades. On the practical side, the design and performance of superconducting magnets are often limited by the suppression of superconductivity in large magnetic fields. The behavior observed in various experiments on superconductors in a magnetic field is quite diverse, and its full elucidation is a substantial scientific challenge. Discovery of the new copper oxide high-temperature superconductors has spurred a significant reexamination of this subject. These materials exhibit phenomena that were not detected in previously studied superconductors. They also have the potential to remain superconducting at much higher magnetic fields than earlier materials and thus may eventually allow the construction of higher field magnets.

New theoretical approaches to the behavior of superconductors in magnetic fields have been explored, based on recently developed concepts in the theory of phase transitions and ordering in condensed matter. Some of this theoretical work is discussed below, but the main focus of this article is on experimental work that explores the behavior of the copper oxide superconductors. These systems exhibit an enormous variety of interesting regimes, many of which have not been carefully studied and only a few of which will be discussed here. The materials can range from those that are highly anisotropic, like $Bi_2Sr_2CaCu_2O_8$ [BSCCO(2212)], to ones that are much less anisotropic, like $YBa_2Cu_3O_7$ [YBCO(123)]; the magnetic fields of interest range from 1 to over $10^5$ G, and the field may be oriented at any angle with respect to the crystalline axes of the material; the temperatures of interest range from a few up to 100 K; and the behavior as a function of the electrical current density in the material is also of much interest.

The authors are at AT&T Bell Laboratories, Murray Hill, NJ 07974.

These materials are type II superconductors, because they can remain superconducting when a magnetic field penetrates the material. (Type I superconductors, on the other hand, lose their superconductivity as soon as the field penetrates.) The basic theory of how type II superconductors behave in a magnetic field was developed by Abrikosov (*1*). He showed that, in type II superconductors, the magnetic field, when greater than the lower critical field, $H_{c1}$, and less than the upper critical field, $H_{c2}$, penetrates the sample in the form of quantized flux lines, each carrying exactly one quantum, $\phi_0 = hc/2e$, of magnetic flux, where $h$ is Planck's constant, $c$ is the speed of light, and $e$ is the electronic charge. The superconducting order parameter, $\Psi$, which is a complex scalar field representing the quantum-mechanical wave function of the paired electrons, has a vortex line for each quantized flux line. If we take $\Psi = |\Psi| \exp(i\phi)$, the magnitude $|\Psi|$ of the order parameter vanishes at the center of each vortex line, whereas the phase $\phi$ changes by $2\pi$ as one makes a full circle around a single vortex line. In the Abrikosov vortex lattice phase of a type II superconductor, these vortex lines, which run parallel to the magnetic field, are arranged in a regular hexagonal crystalline array (as shown in Fig. 1A).

Soon after the discovery of the copper oxide high-temperature superconductors, it was shown that the resistivity in the temperature and magnetic field regime where the Abrikosov vortex lattice was expected to form behaves in a qualitatively different fashion from that found in previously studied type II superconductors (*2*). The reason for the difference, we now know, is that strong thermal fluctuations cause the vortex lattice to melt into a vortex fluid [see, for example, Gammel *et al.* (*3*) and Nelson and Seung (*4*)] well below the temperature at which the local $\Psi$ is driven to zero (Fig. 1B). This contrasts with the phase diagram for conventional superconductors (Fig. 1A), where thermal fluctuations are unimportant. For magnetic fields greater than $H_{c2}$ as estimated within mean-field theory assuming no thermal fluctuations, $H_{c2}^{MF}$, the local $\Psi$ is driven to zero: this is the normal state. In the absence of thermal fluctuations and pinning-induced disorder, the vortex lattice would form for all fields below $H_{c2}^{MF}$. However, in the presence of strong thermal fluctuations, as are important in the copper oxide superconductors, the vortices do form in the vicinity of $H_{c2}^{MF}$ but remain in a strongly fluctuating vortex fluid state down to significantly lower temperatures and fields before freezing. Because of imperfections in the materials, the vortex fluid freezes into a superconducting vortex glass as discussed below. The vortex fluid regime had been known to occur for thin-film superconductors (*5*); the copper oxide superconductors are the first bulk materials for which its existence has become readily apparent. Before discussing why this is the case and what this implies for the materials' resistivity, let us first briefly discuss what happens at much lower fields.

When the magnetic field penetrating a type II superconductor is very small, it penetrates in the form of isolated flux lines, each carrying a vortex line and a quantum, $\phi_0$, of magnetic flux. A cross section of one of these vortex-flux lines reveals two characteristic length scales of the superconductor (*1*): The magnitude of $\Psi$ is significantly suppressed only in the core of the vortex, which is of size $\xi$, the superconducting coherence length. At low temperatures, $\xi$ measures the spatial extent of the Cooper pairs of electrons and is believed to be less than 20 Å for the copper oxide superconductors. This very small coherence length is one thing that makes the copper oxide materials qualitatively different; previously known superconductors generally have much larger coherence lengths. The coherence length grows as the temperature is increased and diverges to infinity at the transition temperature, $T_c$.

The magnetic field in an isolated vortex-flux line is confined by screening currents that circulate around the vortex, with the field intensity decaying exponentially as one moves far away from the flux line, the decay length being the magnetic penetration depth, $\lambda$. This length [$\lambda \gtrsim 1400$ Å for YBCO(123)] far exceeds $\xi$ in the copper oxide superconductors. A superconductor is type II when $\lambda > \xi/\sqrt{2}$; the copper oxide superconductors are strongly type II, that is, $\lambda >> \xi$ or the Ginzburg-Landau parameter $\kappa \equiv \lambda/\xi >> 1$. In the low-field regime the spacing between flux lines $a_0$ is greater than $\lambda$, so the tubes of flux do not strongly overlap. For $\lambda \simeq 1400$ Å this corresponds to fields below 1000 G. When one is well within this regime, the pattern of magnetic flux emerging from the surface of a sample can be imaged by the Bitter decoration technique; results of such studies are described below. The interaction energy between flux lines also decays exponentially with a decay length of 2; for a perfectly clean material the vortex–flux line lattice should then melt at low fields (thus large spacing between flux lines) when this interaction energy, which stabilizes the lattice, becomes too small to withstand the thermal fluctuations of the flux lines. At these low fields the vortex lattice would also be easily disordered by random pinning. This result has been seen in the decoration experiments and is discussed below.

In the high-field regime, the flux lines are strongly overlapping, so that the spacing between them is less than $\lambda$. In this regime the magnetic field in the material is fairly uniform; it remains higher at the vortex cores than in between the vortices, but the difference is smaller than the average field. In the extreme type II limit, this difference is simply proportional to $\phi_0/\lambda^2$. Thus, in this regime, it is not really appropriate any longer to describe the system as one of flux lines. However, the positions of the vortices and their normal cores remain well defined because $a_0 >> \xi$, where $a_0$ is the spacing between vortices.

There are four (not completely unrelated) factors that make the vortex fluid regime in the high-field phase diagram large for the copper oxide superconductors: (i) high temperatures that cause larger thermal fluctuations; (ii) small $\xi$, which allows the vortices to form at a high field $H_{c2}^{MF} \simeq \phi_0/(2\pi\xi^2)$; (iii) large $\lambda$, because the interactions between vortices in this high-field regime are proportional to $1/\lambda^2$ and therefore small; and (iv) strong anisotropy (these layered materials have very anisotropic normal-state conductivity and supercurrent densities, reflecting the fact that the carriers move readily within the copper oxide layers but hop much less readily between layers). The effective mass anisotropy $\Gamma \equiv (m_c/m_a)^{1/2}$ can be at least as high as 200, as compared to 1 in conventional superconductors. This anisotropy results in a reduced interaction between vortices in different copper oxide layers. The reduced interactions here and in (iii) allow larger thermal fluctuations of the vortices.

What do the vortices have to do with the important practical property of a superconductor, namely, its electrical resistivity? For fields below $H_{c2}^{MF}$, the primary source of resistivity is dissipation due to motion of vortices across the current (*6*). Thus, in order for a type II superconductor to have zero resistivity when vortices are present, one must prevent all the vortices from moving. This actually does happen at low enough temperatures because the vortices get pinned to imperfections in the materials. As discussed above, $\Psi$ is suppressed in the core of a vortex. The energy cost of this suppression of the superconductivity depends on the local environment, typically being reduced near chemical or structural imperfections in the material where the superconductivity is weaker. At low temperatures, the vortex will thus tend to get pinned at such places where it has a lower energy.

What effect do such randomly placed pinning centers have on the Abrikosov vortex lattice? Larkin and Ovchinikov (*7*) calculated the resulting distortions of the lattice, showing that the long-range crystalline order of any lattice in less than four dimensions is destroyed by even weak pinning. The resulting vortex pattern should have short-range crystalline order, but the crystalline order is disrupted at long distances. However, as we show below, the lattices can still have quite long-range orientational order. An important question about the resulting pattern is: Are the vortices mobile, resulting in a nonzero resistivity? The answer was believed for many years to be "yes." The total pinning energy for each finite region with short-range vortex lattice order is finite. Thus, if each such region of vortices is assumed to be able to move without consideration of its interactions with other regions, the free-energy barriers, $U_0$, that would have to be surmounted are finite. This assumption leads to a thermally activated resistivity proportional to $\exp(-U_0/k_B T)$ (where $k_B$ is the Boltzmann constant and $T$ is temperature), which may be very small but remains nonzero for all positive temperatures.

However, it has recently been argued by Fisher (*8*) and Fisher, Fisher, and Huse (*9*) that random pinning instead turns the vortex lattice phase into a vortex glass phase, where the vortices are frozen into a particular random pattern that is determined by the details of the pinning in the particular sample being considered. In this vortex glass phase the vortices are not mobile so the ohmic linear resistivity is strictly zero below the phase transition into this phase at a

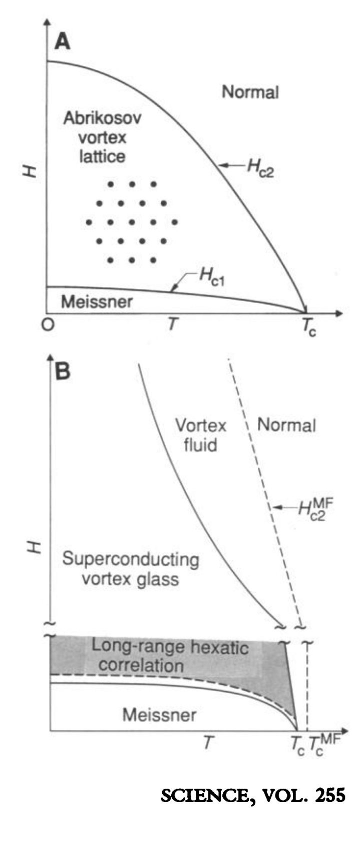


**Fig. 1.** Schematic phase diagrams for clean conventional superconductors where thermal fluctuations and pinning are unimportant (**A**) and for high $T_c$ superconductors where they are important (**B**) as functions of temperature, $T$, and applied magnetic field, $H$. Note that the field scale is broken and highly distorted in (B); for the copper oxide superconductors, $H_{c1}$ ($T$ = 0) is at least several orders of magnitude smaller than $H_{c2}$ ($T$ = 0). The range of stability of the states with long-range hexatic correlations is uncertain. Although they were observed at low temperatures, they may only represent equilibrium near $T_c$, where they were frozen in upon cooling.

temperature $T_g$. The phase is named vortex glass by analogy with the spin glass phase of random magnetic materials and was first introduced for random arrays of Josephson junctions by Shih, Ebner, and Stroud (*10*).

In both the vortex fluid and vortex glass phases, an instantaneous snapshot of the vortex pattern shows no apparent long-range order. However, in the vortex fluid phase the vortex pattern is constantly rearranging, so the correlations between the superconducting order parameter, $\Psi(\mathbf{r})$, at pairs of points in space decay with distance between the two points, vanishing at large distances. In the vortex glass phase, on the other hand, there are long-range correlations between $\Psi(\mathbf{r})$ and $\Psi(\mathbf{r}')$ even for pairs of points $\mathbf{r}$ and $\mathbf{r}'$ that are well separated. These correlations are not in a simple pattern but rather form a static but random pattern that is determined by where all the vortices are located in their frozen configuration. As the vortex glass phase is approached from the vortex fluid phase, these long-range correlations develop continuously, with the vortex-glass correlation length, $\xi_{VG} \sim (T - T_g)^{-\nu}$, where $\nu$ is a critical exponent, diverging as a power of the temperature difference from the transition. The scaling theory of this continuous phase transition has been confirmed in experiments by Koch *et al.* (*11*) and Gammel *et al.* (*12*) on samples of YBCO(123), as discussed below.

Having now briefly summarized some of the theoretical ideas about flux line–vortex patterns and dynamics in type II superconductors, let us now describe some of the recent experiments done on the copper oxide high-temperature superconductors. These experiments are of two basic types: the first directly probe the patterns of magnetic flux either by magnetic decoration or by neutron scattering, whereas the second probe the dynamics by studying the electrical conductivity or other electrodynamic properties of the materials.

In principle, it is possible to study the spatial order of the vortex lattice with neutron diffraction, which has been used to study conventional type II superconductors [Schelten *et al.* (*13*) and Christen *et al.* (*14*)]. In the copper oxide superconductors, the use of neutron diffraction has proven difficult because of the problems of obtaining large single-crystal samples and the fact that the intensity of Bragg scattering from the vortex lines is proportional to the square of the magnitude of the magnetic field contrast in the mixed state, which is very small because of their large London penetration depth $\lambda$. Forgan *et al.* (*15*) detected neutron diffraction from a vortex lattice with $\mathbf{H}\|\hat{c}$ in YBCO(123) and showed that the diffracted signal from the (10) Bragg reflection of the vortex lattice is proportional to $d_{10}\phi_0^2/\lambda^4$, where $d_{10}$ is the (10) plane spacing. Their signals are barely observable over the background from the YBCO(123) and would be smaller by roughly an order of magnitude for BSCCO(2212). Nevertheless, neutron scattering has the potential for studying the order parallel to the vortices as well as perpendicular, can be performed on the same sample as a function of field and temperature, and is a true measurement of bulk properties. For now, we must be content with studying the order of the vortex lattices with direct imaging techniques that do not allow this flexibility.

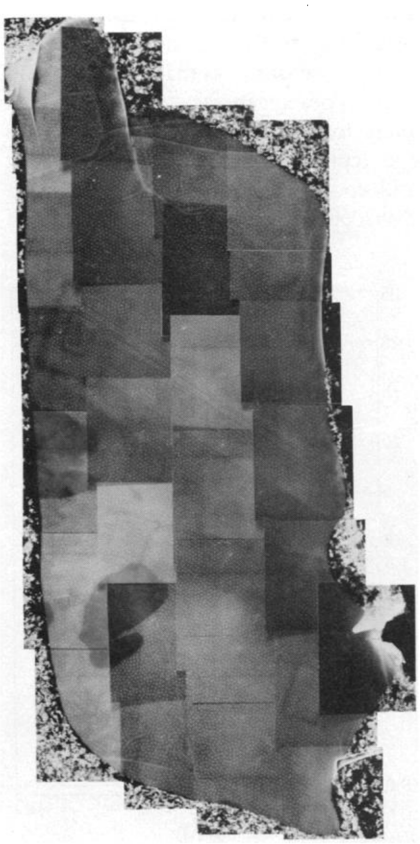

**Fig. 2.** Collage showing the flux lines in a superconducting sample of BSCCO at a field of 8 G and a temperature of 4.2 K. The individual magnetic flux lines are the white spots in the photo. The flux lines were made visible by decoration with magnetic particles, and then they were imaged with an electron microscope. The distance between flux lines is approximately 1.7 μm, and the field is oriented parallel to the *c* axis of the crystal.

## Static Flux-Lattice Structures for Low Temperatures and H$\|\hat{c}$

Direct information on the ordering of the magnetic vortices in the mixed state of the high $T_c$ superconductors can be obtained through the use of the Bitter imaging technique (*16*) in which samples are cooled in an applied magnetic field and subsequently exposed to a smoke of ferromagnetic particles formed by evaporation into a helium buffer gas. The technique was pioneered by Trauble and Essmann (*17*), and Sarma (*18*) to study individual vortices. The ferromagnetic particles travel down magnetic field lines outside the surface of the superconducting sample and form clusters on the surface, which decorate the locations of the vortices. The particles stick to the surface with van der Waals forces. The applied field is then removed, the sample is warmed to room temperature, and the clusters of particles are viewed with an electron microscope.

Direct real-space imaging of the arrangement of individual vortices provides information on both the translational and bond-orientational order of a two-dimensional slice of the vortex lattice as it pierces the sample surface. Present experiments have been limited for the most part to field-cooled samples at $T = 4$ K, subsequently viewed by scanning electron microscopy, for which sufficient contrast is obtained when vortices are separated by roughly $a_0 > 0.3$ μm ($H < \sim 200$ G). Below this separation (or above this field), the ferromagnetic particles have a tendency to form strings by dipole-dipole interaction and the decorated image becomes difficult to interpret. One must take into account the demagnetizing factor of the sample to determine the actual magnetic field in the bulk of the sample. Most of the samples studied to date are thin slabs of ~1 mm extent along the $\hat{a}$, $\hat{b}$ axes and ~5 to 30 μm thickness along $\hat{c}$. The $\hat{a}$ and $\hat{b}$ axes span the copper oxide layers of these materials, while $\hat{c}$ is normal to the layers. For **H** along $\hat{c}$, vortices penetrate the sample at $H \sim 0.5$ G, rather than the measured $H_{c1}$ of ~150 G, owing to this demagnetizing effect. The Bitter decoration technique is limited to a static snapshot of the vortex lattice arrangement in the sample averaged over the time required to decorate—about 1 s. Also, because there is pinning and possibly entanglement of the vortices, the actual temperature during the sample cool-down at which the microscopic arrangement of vortices goes out of equilibrium and freezes into the resulting Bitter pattern is currently unknown. This temperature must lie somewhere between the temperature at which the bulk dc magnetization goes out of equilibrium, $T_{irr}$, which for these low fields is quite close to $T_c$, and the lowest temperature obtained in the decoration experiment, which is 4.2 K.

The Bitter decoration experiments have established the following points about the mixed state of the high $T_c$ superconductors for **H** parallel to $\hat{c}$: (i) the vortices exist as hexagonally correlated, singly quantized vortices with one flux quantum, $hc/2e$, per vortex as in a conventional type II superconductor (*19*); (ii) the vortices undergo pinning at twin boundaries, at crystal defects, and individually at other intrinsic lattice sites in ostensibly defect-free regions (*20*); (iii) in twin-free samples, instead of the long-range translational order expected in the crystalline state of the Abrikosov vortex lattice, the vortex arrangement has short-range translational order with correlation lengths on the order of a few nearest neighbor spacings, but long-range bond-orientational (hexatic) order that extends over ten to several hundred nearest neighbor spacings (*21*); (iv) a rather sharp transition with applied field is observed in BSCCO(2212) between isotropic disorder in the vortex arrangement for $H < 20$ G and hexatic order at higher fields; this transition occurs at considerably lower field ($H \sim 8$ G) for samples that have been annealed in oxygen; for both types of samples the translational and bond-orientational order in the hexatic arrangement increase monotonically with field up to 100 G (*22*); (v) motion of individual vortices comparable to their separation within the 1-s decoration time appears to occur at 15 K in BSCCO(2212), presumably because of thermal motion of the vortices (*23*); (vi) the vortex lattice exhibits the expected ~20% anisotropy from a perfect hexagonal structure in the *a–b* plane in YBCO(123) due to the in-plane effective mass anisotropy of the electrons (*24, 25*) but a smaller anisotropy of ~3 to 10% rather than the nearly 50% expected in BSCCO(2212) from *a–b* mass anisotropy (*21, 22, 24*); (vii) for **H** not parallel to $\hat{c}$, a variety of novel structures have been observed, including oval vortices (*24*) and flux-line chains (*26*).

The advantage of using BSCCO(2212) in the decoration experiments is that excellent quality, untwinned single crystals can be obtained that can be cleaved to expose a clean surface layer for decoration. In addition, the Ginsburg-Landau parameter $\kappa = \lambda/\xi \approx 200$ and the *a–c* carrier mass anisotropy parameter $\Gamma \gtrsim 55$ for BSCCO(2212) make it a rather exotic superconductor. For comparison, YBCO(123) has $\kappa \approx 100$ and $\Gamma \approx 5$, and a conventional type II superconductor such as $Nb_3Sn$ has $\kappa \approx 20$ and $\Gamma = 1$.

A decoration collage of a BSCCO(2212) sample at $H = 8$ G ($\mathbf{H}\|\hat{c}$) is shown in Fig. 2. In that picture one can observe nearly all of the points mentioned above for $\mathbf{H}\|\hat{c}$. Individual vortices of size $hc/2e$ show up as white clusters of particles. They are strongly pinned along stripe defects in the center of the sample [possibly borders between domains in which the $\hat{a}$ and $\hat{b}$ axes are interchanged (*22*)] and there are other obvious sample defects such as surface steps and tears caused by the cleaving procedure. There are dark regions of the sample that exhibit no apparent magnetization or vortices; and vortices show some tendency to align with some sample edges, but not all edges. The sample shows two large uniform interior regions of ~100 by 100 vortices each that are free of obvious sample defects. In our study of the applied field dependence of the order of the vortex arrangement, we have analyzed digitized images from two to three such regions of size ~4,000 vortices for each of 20 decorated samples. Some studies have examined regions of as many as 15,000 vortices.

In Fig. 3, A through C, are shown defect maps known as Delaunay triangulations of the arrangement of roughly 4000 vortices from three different BSCCO samples cooled to 4 K in fields parallel to $\hat{c}$ of 69, 23, and 8 G, respectively (*22*). These samples had been previously annealed at 600°C for ~24 hours in 1-atm oxygen and then quenched to room temperature. Indications are that the oxygen annealing process probably does not greatly affect either $\kappa$ or $\Gamma$ when compared to those of the as-made samples (*27*) but does reduce the concentration of oxygen vacancies (*28*), which could serve as pinning centers for vortices. In the defect maps shown, each vortex center is represented as a vertex of nearest neighbor bonds. Non-sixfold–coordinated centers, defects in a perfect hexagonal array, are shaded in the figure. The vortices are

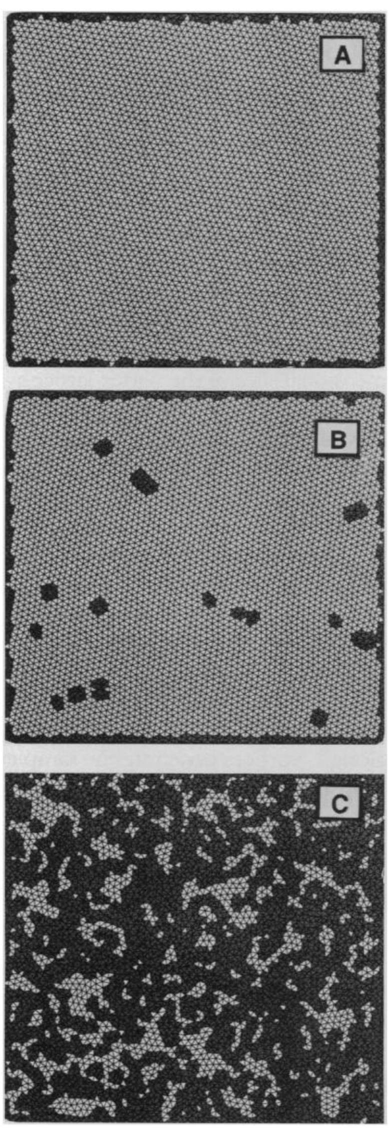


**Fig. 3.** Delaunay triangulations for image-processed scanning electron micrographs of Bitter decorated, oxygen-annealed BSCCO crystals cooled to 4.2 K in magnetic fields of 69, 23, and 8 G, respectively. The fields of view are (**A**) 27 by 25 $\mu m^2$, (**B**) 48 by 45 $\mu m^2$, and (**C**) 72 by 68 $\mu m^2$. Shaded triangles join vertices that are not sixfold-coordinated.

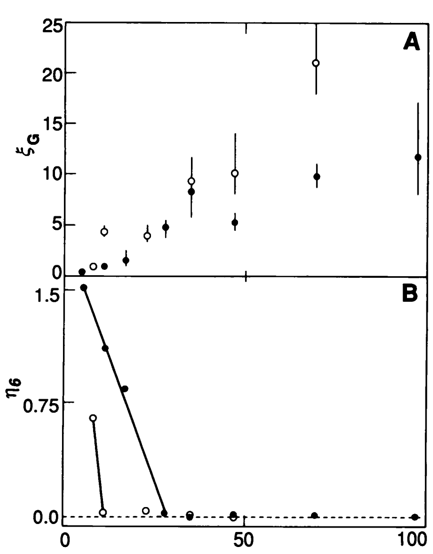


**Fig. 4.** (**A**) The translational correlation lengths $\xi_G$ for annealed (open) and as-made (closed) samples in units of nearest neighbor spacings. (**B**) The bond-orientational correlation exponents $\eta_6$. The line at $\eta_6 \approx 0.06$ is our limit of experimental resolution.

quite disordered at 8 G, whereas much less so at 23 G, and no defects in the vortex lattice are visible in the field of view at 69 G. The translational correlation length $\xi_G$, as determined from exponential fits to the correlation function of the translational order parameter of the vortex lattice $\Psi_G(\mathbf{r}) = \exp(i\mathbf{G}\cdot\mathbf{r})$, where $\mathbf{r}$ is a vortex position, is shown versus $H$ in Fig. 4A for both annealed and as-made (unannealed) samples. A monotonic increase of $\xi_G$ from $\sim 2\ a_0$ at 5 G to $\sim 20\ a_0$ is observed for the annealed samples, whereas the as-made samples have $\xi_G$ roughly half that value at each field.

In the 69-G and 23-G defect maps (Fig. 3, A and B) one can easily sight down rows of vortices, despite the relatively small value of $\xi_G$ compared to the size of the image. This is the signature of a hexatic, which exhibits short-range translational order and long-range bond-orientational order (*29–31*). The bond-orientational order of the vortex lattice is characterized by an order parameter $\Psi_6(\mathbf{r}) \equiv \exp[i6\theta(\mathbf{r})]$. The correlation function of this bond-orientational order parameter measures the correlation of a bond angle $\theta(\mathbf{r})$ at $\mathbf{r}$ (modulo $2\pi/6$) with that at the origin. Assuming a power law dependence for the decay of correlations of the form $\langle\Psi_6^*(0)\cdot\Psi_6(\mathbf{r})\rangle \sim r^{-\eta_6}$, one can extract a correlation exponent, $\eta_6$, from fits to computed bond-orientational correlation functions from the measured position of vortex centers (*32*). The exponents are shown for the same series of decorations in Fig. 4. Immediately obvious from the figure is the abrupt change of the fitted $\eta_6$ from a relatively large value of 0.8, a rather steep decay of the bond-orientational order, to the limits of the experimental resolution, 0.06, where it does not decay at all to within our experimental resolution. The change occurs rapidly in a change in the applied field of only a few gauss, but for different fields for the as-made and annealed samples, presumably reflecting the change in the concentration of intrinsic pinning sites in the two types of samples. This abrupt change in the bond-orientational order with $H$ is difficult to reconcile with theories that include only a range of pinning energies but no phase transition. These data are consistent with the predictions of an isotropic vortex fluid–hexatic vortex glass (*8, 9, 31*) or hexatic vortex fluid phase transition (*33*) or a transition between a strongly pinned disordered glassy phase to a less strongly pinned hexatic near $H_{c1}$ (*34*). Experimental data on vortex mobility versus temperature and the microscopic irreversibility temperature versus $H$ in this field range are needed to discriminate among the various possibilities.

## Flux-Line Lattice Structures for Other Field Orientations

Decoration experiments can also be performed with the magnetic field applied at an angle with respect to the $\hat{c}$ axis. In the experiments to be discussed here, all the samples were mounted at a fixed angle $\theta$ with respect to the field and field-cooled with all decorations having been done at 4.2 K. For these orientations a variety of novel structures have been seen, including flux-line chains (*24*) and oval vortices (*26*).

In BSCCO(2212) there have been a variety of results. The first measurements we will discuss were of the average density of vortices on the cleaved face ($\perp$ to $\hat{c}$) of the crystal as a function of angle (*26*). For all angles up to 85° the average density was found to follow a $(B/\phi_0)\cos\theta$ dependence. In other words, the vortex lattice on the surface is only induced by the component of the magnetic field $\mathbf{B}$ parallel to $\hat{c}$. This dependence had been inferred by Kes *et al.* (*35*) through an analysis of torque magnetometer data.

The vortex lattice structures seen on the surface of BSCCO(2212) fall into two regimes, $\theta < 60°$ and $\theta > 60°$. For the smaller angles, the vortex lattice present on the surface of the sample is isotropic, to within the 5 to 10% distortions discussed above. In addition, there is no apparent preferred orientation of the flux lattice, either with respect to the sample's crystallographic axis or with respect to the magnetic field's tilt axis. Interestingly enough, this measured isotropy implies an extreme anisotropy in the penetration depth or effective mass. To clarify this point, consider the case of an isotropic system. In the absence of surface effects, a hexagonal vortex lattice will form with the vortex lines parallel to the applied field. When the field is not perpendicular to the decorated surface, the resulting pattern seen is a distorted lattice, with a distortion factor $\rho \equiv 1/\cos\theta$. In the limit of large anisotropy $\Gamma \to \infty$, however, the distortion of the hexagonal vortex lattice in the bulk predicted from the anisotropic London equations is likewise $1/\cos\theta$ (*36*). This exactly cancels the distortion in the surface pattern due to the tilted field, and the observed vortex lattice will then be isotropic. Assuming a maximum experimentally measured distortion of 5% at 60°, we find that a limit of $\Gamma^2 > 8$ can be placed on the effective mass ratio using the full form of the London equations. Although this is certainly consistent with torque magnetometry (*37*) and resistivity, which give $\Gamma \sim 60$ to 200, this analysis is insensitive to the value of $\Gamma$ when the anisotropy is large.

For angles $\theta > 60°$, a dramatic new structure emerges (Fig. 5). An array of flux chains lies in the plane spanned by $\mathbf{B}$ and $\hat{c}$. The chains have an increased line density of vortices with respect to the background lattice. The chains also orient the intervening lattice so that one of the lattice vectors is parallel to the chain direction and perpendicular to the tilt axis. This is very different from the case for $\theta < 60°$ where no preferred orientation of the lattice is seen. Independent of the crystallographic $\hat{a}$-axis direction, this is the direction selected by London theory (*36*), although without having included or predicted the chains that are so prominent in the picture. This orientation was not defined before the appearance of the chains. It has been widely reported that neutron scattering experiments are consistent with a lattice rotated 90° from this. Actually, this is based on three results, technectium (*13*), YBCO (*15*), and $UPt_3$ (*38*). In all three cases, the field orientation corresponded to $\theta = 90°$, in which special case the two lattice orientations are again degenerate within the anisotropic London equations. The decoration results presented here represent the first true test of this prediction of the flux lattice orientation as a complete function of tilt angle.

We can further analyze the photo shown in Fig. 5. In the plane of the photograph, we can let the spacing between vortices along the chain be $D$ and that between chains be $C$. Although $C$ has large variations due to the chain wandering which can be seen in Fig. 5, both $D$ and $C$ are found to scale as $B^{-1/2}$ at a fixed angle. Because this is the same scaling as the vortex lattice constant, the picture at a fixed angle is field-independent in the sense that the field only sets the overall magnification, not the structure we see. For all fields and angles studied, we find $DC \propto \phi_0/B$. If the chain structure is interpreted as a superlattice modulation, this scaling is equivalent to

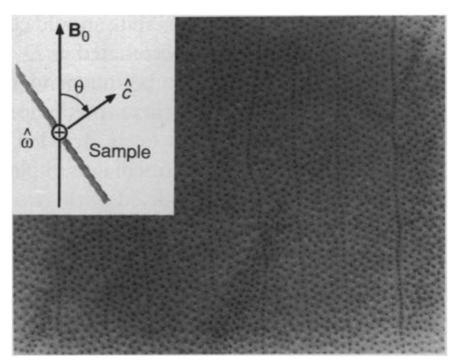


**Fig. 5.** A region of a decorated BSCCO crystal is shown with field of 35 G applied at an angle of 70° from the $\hat{c}$ axis. The face decorated is normal to the $\hat{c}$ axis. The dark dots are the vortices with an average spacing of 1.4 μm. The chains run approximately perpendicular to the rotation axis and define the orientation of the vortex lattice between chains. (The field of view is 75 μm by 60 μm.)

**Fig. 6.** Decoration of a face parallel to the $\hat{c}$ axis on the edge of a YBCO crystal at a field of 8 G. The arrow marks a twin boundary and is also the $\hat{c}$ direction. Note the oval vortices [from (*24*)].

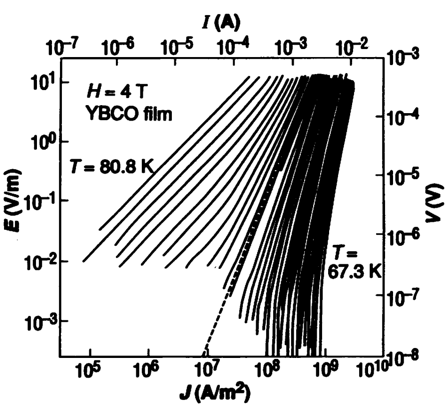


**Fig. 7.** Current-voltage curves for a YBCO film at an applied field of 4 T (1 T = $10^4$ G) for temperatures from 80.8 to 67.3 K at intervals of 0.3 K. The temperature for $T_g$ at this field is shown as a dotted line. [Adapted from (*11*)]

incorporating one extra flux quantum per superlattice unit cell. A necklace of dislocation pairs, with zero net Burgers vector, dresses the chains to accommodate the extra flux line. These dislocations can be identified in a Delaunay triangulation of the overall structure.

As the tilt angle increases toward 90°, the number of Abrikosov vortices between chains decreases. Owing to the large fluctuations in $C$, the exact form of this reduction is difficult to state quantitatively. One form, consistent with the data, arises from considering distortions of an isotropic lattice. In this case, $D = 0.75(\phi_0/B \cos \theta)^{+1/2}$. Experimentally, the number of lattice constants between chains varies from 11 at 60° to 2 at 85°.

Flux-line chain structures were anticipated theoretically (*39, 40*), although significantly different in detail from our results. It is clear experimentally that the chains are formed by at least a weakening of the repulsive vortex-vortex interaction in the plane formed by **B** and $\hat{c}$. Considering the enormous anisotropy, this is presumably related to the current paths, which tend to stay in the $\hat{a}$–$\hat{b}$ plane, independent of field orientation. Calculations have centered on the effective mass approximation. Such theories suggest that, near $H_{c1}$, a vortex-vortex attraction develops for extreme anisotropy in tilted fields. This is a result of the current paths remaining in the planes and the simple observation that two dipoles attract when their axes are both parallel and along the line connecting them. Extensions of these theories have shown that this state should consist of chains only. The spacing along the chains is estimated as $D = (\lambda_a\lambda_b\lambda_c)^{1/3} \sim 0.8$ μm. Further, this is predicted to be independent of field. Our observations contradict both of these predictions. Recently, the finite thickness of the sample has been included in the theory (*41*). The lowest energy state for intermediate sample thicknesses appropriate to this experiment was modeled with two types of vortices, chain vortices parallel to **B** and a hexagonal lattice parallel to $\hat{c}$. Although the ratios of these two types of vortices appear to be consistent with our results, again the calculations do not reproduce the field dependence of the experiments. It may be that nonlocalities are playing an important role. Further simulations with the nonlocal expressions are now in progress to model the results (*41*).

Dolan *et al.* (*24*) were able to decorate the surface perpendicular to the $\hat{a}$–$\hat{b}$ plane in YBCO(123). A dramatically distorted lattice (Fig. 6) was seen. It can be explained by assuming a mass ratio of $\Gamma^2 = 30$. This mass ratio is in rough agreement with other estimates (*42*). The oval structure of the individual vortices can be similarly explained. The pattern in Fig. 6 is strongly influenced by the presence of a twin domain boundary that aligns one chain (marked with an arrow). The rapid degradation of the order may be due to the weak shear modulus (*43*), reduced by a factor $\Gamma^4 \approx 900$, in this direction combined with a small flux gradient.

We conclude from the above that the mixed state of extremely anisotropic superconductors is important to the understanding of transport and noise in the high-$T_c$ superconductors, as well as other layered systems. Images such as those we have presented here are one road to this goal.

## Vortex Dynamics

Up until now we have been discussing static structures of the vortex–flux-line lattices in these materials. We will now discuss the dynamics. Early evidence for unconventional behavior of the vortex dynamics in these materials came from measurements of the decay of magnetization in ceramic LaSrCuO (*44*). In those experiments, an irreversibility line was found that has been taken as evidence for thermally activated depinning of the vortex lines (*45, 46*). This is a fundamentally single-particle view of the dynamics. The basic idea is that either individual vortex lines or bundles of small numbers of vortex lines are thermally activated over pinning barriers, which are present in the sample as a result of disorder. In this picture, the resistivity should be thermally activated with the functional form $\exp(-U_0/k_BT)$, which is nonzero at all nonzero temperatures.

A different and more controversial point of view was put forth as a result of subsequent high $Q$ (high quality factor) mechanical oscillator measurements by Gammel *et al.* on single crystals of YBCO and BSCCO (*3*). These experiments suggested that the irreversibility line actually reflects a vortex lattice melting transition from a low-temperature ordered phase into a high-temperature vortex fluid. The high temperatures, short coherence lengths, and large $\hat{c}$-axis anisotropies were postulated to increase the importance of thermal fluctuations to allow a vortex lattice melting transition similar to that both predicted and found in two-dimensional films (*5, 47*). It was also suggested (*3*) that a Lindemann criterion for vortex lattice melting (*48, 49*) could satisfactorily explain the transition temperatures found in these systems.

The melting or phase transition picture takes the point of view that many-body effects are crucially important and must be taken into account if one is to understand the statics and dynamics of the vortex arrays in these systems. In this picture there must be a low-temperature ordered phase with a broken symmetry, which then undergoes a phase transition into a high-temperature disordered vortex fluid phase. This transition is driven by thermal fluctuations. As discussed previously, one such candidate ordered ground state with long-range orientational order but short-range positional order has been found in recent low-field decoration experiments.

During the ensuing controversy about the melting idea, it was correctly pointed out that the simple idea of melting fails to take into account the disorder in the lattice that must be present as a result of random pinning of the flux lines. However, more recently theories that do include pinning disorder but also find a phase transition have evolved. Following the work of Shih, Ebner, and Stroud (*10*), Fisher, Fisher, and Huse (*9*) postulated a vortex glass transition. In this picture the vortices at low temperatures are frozen into a particular random configuration as determined by the details of the pinning centers in the specific sample. In the vortex glass phase, the vortices are not free to move and so the ohmic linear resistivity is strictly zero. Koch *et al.* (*11*) found evidence for such a transition on YBCO films. Figure 7 is an example of their data used to argue for a vortex glass phase transition. Shown are current-voltage (*I-V*) data as a function of temperature at a fixed field of 4 T (1 T = $10^4$ G). Koch *et al.* found a crossover on cooling from ohmic to power-law to exponential *I-V* curves as predicted by the vortex glass theory. However, claims were made that the data could still be fit by conventional, thermally activated behavior (*50, 51*). Recent measurements by Gammel, Schneemeyer, and Bishop (*12*) with picovolt sensitivity on YBCO(123) single crystals with roughly six orders of magnitude greater sensitivity than the previous measurements provided even more compelling support for the vortex glass phase transition.

In the vortex glass model there is a true phase transition at $T_g$, between vortex fluid and vortex glass phases. Associated with this transition there is a diverging correlation length (*52*) given by $\xi_{VG} \sim (T - T_g)^{-\nu}$ and a diverging correlation time $\tau \sim \xi_{VG}^{z}$. The vortex glass model makes several predictions about the resistivity as a function of temperature, magnetic field, and current for a three-dimensional type II superconductor near this phase transition. The first prediction is that the linear response resistivity $R$ should vanish near $T_g$ as $R \sim (T - T_g)^{+(z-1)\nu}$. The second prediction is that the current scale for nonlinear response should vary as $J_{sc} \sim (T - T_g)^{2\nu}$. The physical idea for this vanishing current scale for nonlinear response is as follows: the measuring current defines a length scale by $L \sim (ck_BT/\phi_0 J)^{1/2}$. This is the length scale below which the effects of current on the thermal distributions of vortices are linear. In order to remain in the linear response regime, we must have $L > \xi_{VG}$. The response goes nonlinear at a current density $J_{sc}$ where $L \sim \xi_{VG}$. As $T \rightarrow T_g$ the correlation length, $\xi_{VG}$, diverges to infinity and the current scale for linear response therefore vanishes.

The alternative point of view, that of thermally activated flux flow (TAFF), says that the resistance should go as $R \sim R_0\exp(-U_0/k_BT)$ and that the current scale for linear response should be proportional to $T$. It was our reasoning that measurements at and near linear response at the picovolt level would provide the biggest testable differences between the various theories. To that end, we built a special squid picovoltmeter that allowed us to measure *I-V* curves in magnetic fields up to 6 T with subpicovolt sensitivity. Our measurements of the temperature dependence of both $R$, the linear response resistivity, and the onset of nonlinear response strongly constrain theoretical fitting parameters and have allowed us to rule out the class of models that attempt to explain the dynamics in these systems as due solely to thermally activated hopping over barriers. Figure 8 is a log-log plot of $R$ and the current scale for linear response $J_{sc}$ for a YBCO(123) single crystal at a field of 6 T. Both quantities vanish as powers of $(T - T_g)$ with $T_g$ = 74.0 K. In any TAFF model, such behavior for the linear resistivity and the current scale for linear response is impossible to obtain. In a TAFF model both quantities are only singular at $T$ = 0. For example, in Fig. 8 TAFF models

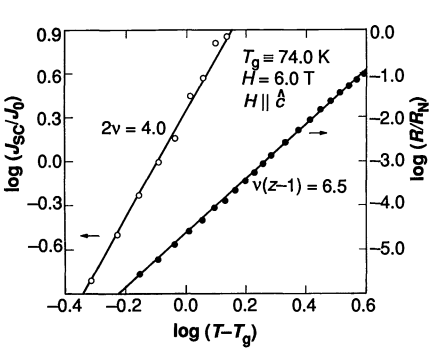


**Fig. 8.** Linear resistivity $R$ and the current scale for linear response $J_{sc}$ versus the reduced temperature $(T - T_g)$ on a log-log plot for a YBCO(123) single crystal at an applied field of 6 T. The straight lines are the fits to the scaling theory for the vortex glass phase transition.

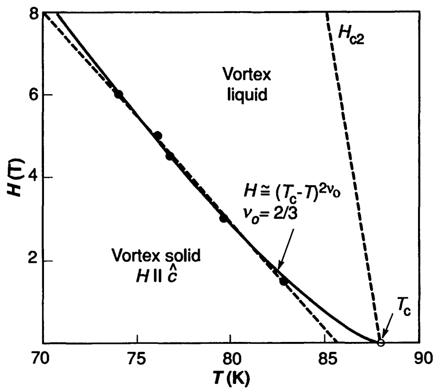


**Fig. 9.** Phase diagram taken from the picovolt measurements on a YBCO crystal. $H_{c2}$ is taken from estimates of Welp *et al.* (*54*). The solid line is a 4/3 power-law fit to the data, and the dashed line is a linear fit.

would predict $J_{sc}$ to be an essentially horizontal straight line on the scales shown here. These TAFF predictions are clearly at odds with the data. From measurements such as shown in Fig. 8 we can obtain the critical exponents for the vortex glass phase transition: we obtain $\nu = 2.0 \pm 1$ and $z = 4.5 \pm 1.5$ for YBCO(123) single crystals in agreement with the earlier thin film data (*11*).

Shown in Fig. 9 is a composite phase diagram for the high-field vortex state of single-crystal YBCO(123). The solid points are transition temperatures $T_g$ as extracted from superconducting quantum interference device (SQUID) picovoltmeter data of the kind shown in Fig. 8. The $H_{c2}$ line represents where the transition would be if one could neglect thermal fluctuations. The prediction of the vortex glass model for the phase transition is shown as the solid line. A linear $T_g$ versus $H$ shown as the dashed line fits just as well as the $H_g \sim (T_c - T_g)^{4/3}$ expected as a result of strong critical fluctuations. The low-field behavior of the phase boundaries is both theoretically and experimentally an open question. For example, it is not now clear how the low-field phase boundary seen in decoration experiments (Fig. 4) should join the phase transition line as measured with high-field probes such as the picovoltmeter (Fig. 9). This is still an open question.

At the moment, results on YBCO(123) films (*11*), YBCO(123) single crystals (*12*), and single crystals of BSCCO(2212) (*53*) show convincing proof of the type shown above for the vortex glass model. It is worthwhile pointing out why so many workers in the field find "evidence" for thermal activation models and fail to see the vortex glass phase transition. In the best of circumstances, it is experimentally hard to tell the difference between a large power law and an exponential law for the resistivity versus temperature. In order to do so, one needs to be able to follow the dependence over a wide range. Experiments that probe the system either at too high a current level or in ceramic materials that cut off the diverging vortex glass correlation length at the grain size will never be able to see the transition. This does not mean that it does not exist, merely that most experiments will not be able to probe it. For example, in BSCCO(2212), in a field of 3 T, the vortex glass critical region corresponds to a typical sample resistance of $10^{-7}$ ohm and below. With typical measuring currents of 1 mA and below to avoid sample heating, one finds that voltage sensitivities of $10^{-10}$ V and better are needed to probe the critical region. This is far outside the voltage sensitivity of most experiments. Thus, many conventional experiments do not have the sensitivity to probe the vortex glass transition. However, it is important to remember that in experimental physics the absence of proof should not be confused with the proof of absence.

## Conclusions

The implications of the data presented here are significant. For a long time it was believed that in a magnetic field the resistance of a type II superconductor only became strictly zero at $T = 0$. We now know that there exists a finite temperature phase transition at high fields at which the resistance becomes zero. The low-temperature ordered phase is a superconducting vortex glass, which at very low fields has quite long-range orientational (hexatic) order. We are slowly making real progress in our understanding of the vortex–flux lattice statics and dynamics. The oxide superconductors have proven to be a wonderful testing ground for our understanding in this area and have forced us to reexamine, extend, and in some cases discard certain theoretical models. There remain many unanswered questions. These include the role of anisotropy, a microscopic understanding of the critical currents in these systems, and the behavior of the lattices in the very clean limit.

REFERENCES AND NOTES


1. For a review, see A. L. Fetter and P. C. Hohenberg, in *Superconductivity*, R. D. Parks, Ed. (Dekker, New York, 1969), vol. 2, pp. 817–920.
2. B. Oh *et al.*, *Phys. Rev. B* **37**, 7861 (1988).
3. P. L. Gammel, L. F. Schneemeyer, J. V. Waszczak, D. J. Bishop, *Phys. Rev. Lett.* **61**, 1666 (1988); D. J. Bishop, *Bull. Am. Phys. Soc.* **33**, 606 (1988).
4. D. R. Nelson and H. S. Seung, *Phys. Rev. B* **39**, 9153 (1989).
5. D. S. Fisher, *ibid.* **22**, 1190 (1980); P. L. Gammel, A. F. Hebard, D. J. Bishop, *Phys. Rev. Lett.* **60**, 144 (1988).
6. Y. B. Kim and M. J. Stephen, in *Superconductivity*, R. D. Parks, Ed. (Dekker, New York, 1969), vol. 2, pp. 1107–1162.
7. A. I. Larkin and Yu. N. Ovchinikov, *J. Low Temp. Phys.* **34**, 409 (1979).
8. M. P. A. Fisher, *Phys. Rev. Lett.* **62**, 1415 (1989).
9. D. S. Fisher, M. P. A. Fisher, D. A. Huse, *Phys. Rev. B* **43**, 130 (1991).
10. W. Y. Shih, C. Ebner, D. Stroud, *ibid.* **30**, 134 (1984).
11. R. H. Koch *et al.*, *Phys. Rev. Lett.* **63**, 1511 (1989).
12. P. L. Gammel, L. F. Schneemeyer, D. J. Bishop, *ibid.* **66**, 953 (1991).
13. J. Schelten, G. Lippmann, H. Ullmaier, *J. Low Temp. Phys.* **14**, 213 (1974).
14. D. Christen, K. Kerchner, S. T. Sekula, *Phys. Rev. B* **21**, 102 (1980).
15. E. M. Forgan *et al.*, *Nature* **343**, 735 (1990).
16. For a review, see R. P. Huebner, *Magnetic Flux Structures in Superconductors* (Springer-Verlag, Berlin, 1979).
17. H. Trauble and U. Essmann, *J. Appl. Phys.* **39**, 4052 (1968).
18. N. V. Sarma, *Philos. Mag.* **17**, 1233 (1968).
19. P. L. Gammel *et al.*, *Phys. Rev. Lett.* **59**, 2952 (1987).
20. G. J. Dolan *et al.*, *ibid.* **62**, 827 (1989).
21. C. A. Murray *et al.*, *ibid.* **64**, 2312 (1990).
22. D. G. Grier *et al.*, *ibid.* **66**, 2270 (1991).
23. R. N. Kleiman *et al.*, *ibid.* **62**, 2331 (1989).
24. G. J. Dolan, F. Holtzberg, C. Field, T. R. Dinger, *ibid.*, p. 2184.
25. L. Ya. Yinnikov, J. V. Grigoriera, L. A. Gurevich, Yu. A. Ossipyan, in *High Temperature Superconductivity from Russia*, A. I. Larkin and N. V. Zavaritsky, Eds. (World Scientific, London, 1989), pp. 171–180.
26. C. A. Bolle *et al.*, *Phys. Rev. Lett.* **60**, 112 (1991).
27. S. Martin, personal communication.
28. F. Parmigiani *et al.*, *Phys. Rev. B* **43**, 3085 (1991).
29. B. I. Halperin and D. R. Nelson, *Phys. Rev. Lett.* **41**, 121 (1978).
30. D. R. Nelson, M. Rubinstein, F. Spaepen, *Philos. Mag. A* **46**, 105 (1982).
31. E. M. Chudnovsky, *Phys. Rev. B* **40**, 11355 (1989).
32. For a review, see D. R. Nelson, in *Phase Transitions and Critical Phenomena*, C. Domb and J. L. Lebowitz, Eds. (Academic Press, London, 1983), vol. 7, pp. 1–99.
33. M. C. Marchetti and D. R. Nelson, *Phys. Rev. B* **41**, 1910 (1990).
34. D. R. Nelson and P. LeDousal, *ibid.* **42**, 10113 (1990).
35. P. H. Kes *et al.*, *Phys. Rev. Lett.* **64**, 1063 (1990).
36. L. J. Campbell, M. M. Doria, V. G. Kogan, *Phys. Rev. B* **38**, 2439 (1988).
37. D. E. Ferrell *et al.*, *Phys. Rev. Lett.* **63**, 782 (1989).
38. R. N. Kleiman *et al.*, in preparation.
39. A. M. Grishin *et al.*, *Sov. Phys. JETP* **70**, 1089 (1990).
40. A. J. Buzdin and A. Yu. Simonov, *JETP Lett.* **51**, 191 (1990).
41. L. Daemon and L. J. Campbell, *Bull. Am. Phys. Soc.* **36**, 1064 (1991).
42. L. Krusin-Elbaum, A. P. Malozemoff, Y. Yeshurun, D. C. Cronmeyer, F. Holtzberg, *Phys. Rev. B* **39**, 2936 (1989); L. Krusin-Elbaum, R. L. Greene, F. Holtzberg, A. P. Malozemoff, Y. Yeshurun, *Phys. Rev. Lett.* **62**, 217 (1989).
43. V. G. Kogan and L. J. Campbell, *Phys. Rev. Lett.* **62**, 1552 (1989).
44. K. A. Muller, M. Takashige, J. G. Bednorz, *ibid.* **58**, 1143 (1987).
45. A. P. Malozemoff *et al.*, *Phys. Rev. B* **38**, 6490 (1988).
46. Y. Yeshurun and A. P. Malozemoff, *Phys. Rev. Lett.* **60**, 2202 (1988).
47. B. A. Huberman and S. Doniach, *ibid.* **43**, 980 (1979).
48. A. Houghton, R. A. Pelcovits, S. Sudbo, *Phys. Rev. B* **40**, 6763 (1989).
49. M. A. Moore, *ibid.* **39**, 136 (1989).
50. R. Griessen, *Phys. Rev. Lett.* **64**, 1674 (1990).
51. S. N. Coppersmith, M. Inui, P. B. Littlewood, *ibid.*, p. 2585.
52. Here we assume that the scaling is isotropic, that the correlation length along the magnetic field diverges with the same critical exponent as that perpendicular to the field. If this is not the case, the scaling of the resistivity and current will be a little more complicated. For YBCO, where the pinning might be predominantly from spatially extended flat twin boundaries, such anisotropic scaling might arise when the field is parallel to the twins, as has been discussed by D. Nelson [in *Phenomenology and Applications of High Temperature Superconductivity*, K. Bedell and M. Inui, Eds. (Addison-Wesley, Reading, MA, in press)].
53. H. Safar, P. L. Gammel, D. J. Bishop, D. B. Mitzi, A. Kapitulnik, in preparation.
54. U. Welp *et al.*, *Phys. Rev. Lett.* **62**, 1908 (1989).


55. We thank D. Nelson, P. Littlewood, C. Varma, T. Palstra, and B. Batlogg for many helpful discussions, and we acknowledge fruitful collaborations with D. Fisher, M. P. A. Fisher, C. Bolle, G. Dolan, D. Grier, A. Kapitulnik, R. Kwo, D. Mitzi, and L. Schneemeyer.


# Paleoceanography of the Tropical Eastern Pacific Ocean


RICHARD W. GRIGG AND RICHARD HEY



**The East Pacific Barrier (EPB) is the most effective marine barrier to dispersal of tropical shallow-water fauna in the world today. The fossil record of corals in the eastern Pacific suggests this has been true throughout the Cenozoic. In the Cretaceous, the EPB was apparently less effective in limiting dispersal. Equatorial circulation in the Pacific then appears to have been primarily east to west and the existence of oceanic atolls (now drowned guyots) in the eastern Pacific probably aided dispersal. Similarly, in the middle and early Mesozoic and late Paleozoic, terranes in the central tropical Pacific likely served as stepping stones to dispersal of tropical shelf faunas, reducing the isolating effect of an otherwise wider Pacific Ocean (Panthalassa).**


THE TROPICAL EASTERN PACIFIC OCEAN HAS BEEN DESCRIBED as the most effective barrier to dispersal of warm-water shelf fauna in the world (*1*). Ekman named this body of water the East Pacific Barrier (EPB) and defined it as that expanse of ocean where no islands exist in the tropical Pacific separating the Indo–West Pacific (IWP) zoogeographic province from the eastern Pacific province (Fig. 1). Charles Darwin described it as an "impassable barrier" for the migration of coastal marine species (*2*). In terms of coral reef habitats, the EPB exists between the Line Islands in the western Pacific and the western coast of the Americas and several offshore islands in the eastern